Separation of Spin and Charge Transport in pristine π-Conjugated Polymers

Formatted: Font color: Auto

Matthew Groesbeck[†], Haoliang Liu[†], Marzieh Kavand, Evan Lafalce, Jingying Wang, Xin Pan Taniya-Hariska Teanahewa, Henna Popli, Hans Malissa, Christoph Boehme, Z. Valy Vardeny^{*} Department of Physics & Astronomy, University of Utah, Salt Lake City, UT 84112, USA.

Formatted: Font: (Default) Times New Roman, 12 pt

Formatted: Font: (Default) Times New Roman, 12 pt, Font color: Auto

Formatted: Font: (Default) Times New Roman, 12 pt

Formatted: Font: (Default) Times New Roman, 12 pt

Formatted: Font color: Auto

Formatted: Font: (Default) Times New Roman, 12 pt, Font color: Auto

We have experimentally tested whether the spin-transport and charge-transport in pristine π -conjugated polymer films at room temperature, proceed via the same electronic processes. We have obtained the spin diffusion coefficient of several π -conjugated polymer films from the spin diffusion length measured by the technique of inverse spin Hall effect and the spin relaxation time measured by pulsed electrically detected magnetic resonance spectroscopy. In parallel, the charge diffusion coefficient was obtained from the time-of-flight mobility measurements on the same films. We found that the spin diffusion coefficient is larger than the charge diffusion coefficient by about one to two orders of magnitude, and conclude that spin and charge transports in disordered polymer films occur through different electronic processes.

Formatted: Font color: Auto

†These authors have contributed equally to this work.

*Correspondence to: val@physics.utah.edu.

Organic semiconductors (OSEC) have been studied extensively, not only because of their versatility for electronic and optoelectronics applications such as organic light emitting diodes¹, transistors² and solar cells³, but also for their potential applications in spintronics^{4–8}. OSEC are predominantly made of light atoms with low atomic numbers, and therefore, the electronic states in OSEC typically exhibit weak spin-orbit coupling (SOC), which may lead to long spin relaxation times. This suggests potential applications as spin transport materials in spintronics devices^{9,10}. Indeed, for more than a decade, OSEC have been demonstrated to work as efficient buffer layers in spin-valve structures, sandwiched between two ferromagnetic (FM) electrodes

Formatted: Font: (Default) Times New Roman, 12 pt

Formatted: Font: (Default) Times New Roman, 12 pt

with different coercivities, 4,9,11 which serve as injector/detector pair of both a spin-polarized current as well as an electrical current under application of a bias voltage at cryogenic temperatures.

More recently, the transport of pure spin current (in absence of charge current) through OSEC has been demonstrated using spin pumping via ferromagnetic resonance (FMR) of a FM substrate at room temperature¹². In this technique, the spin current in the OSEC layer is launched through scattering of FMR-induced magnons at the FM/organic interface, which serves as a spin transport layer. The detection of the pure spin current is possible through observation of a SOCinduced electric current which is transverse to the pure spin current, the so-called inverse spin Hall effect (ISHE)¹³. Pure spin currents in OSC layers have been demonstrated with the ISHE by using both non-magnetic detector layers with strong SOC, or directly through the weakly SOC organic transport layers themselves 14-16. The latter approach was first demonstrated by using a bilayer structure consisting of the ferrimagnetic insulator namely Y₃Fe₅O₁₂ and the conducting polymer PEDOT:PSS¹⁴, while the former has been accomplished using trilayer structures comprised of an FM injector layer, OSEC transport layer, followed by an ISHE detector layer with strong SOC, typically Pt or Pd. These trilayer structures have since been used to obtain spin diffusion lengths of various OSEC interlayers 17-21. Importantly, using pure spin current and the ISHE for its detection circumvents the well-known problem in spintronics applications of impedance mismatch that rely on injection of spin-aligned carriers into the non-magnetic layer.22,23

Charge transport in OSEC has been studied extensively in the past, and is generally considered to be well understood for most materials in this class of materials. Within disordered OSEC such as π -conjugated polymers or small molecules, the charge transport is governed by transitions between localized electronic states, such as hopping or tunneling²⁴. In contrast, spin transport and spin relaxation mechanism in OSEC have been studied to a lesser degree. For localized electronic states, various physical processes may affect both spin transport and spin relaxation, including interaction with nuclear spin states (hyperfine interaction)^{25,26} and SOC^{27,28}. For instance, spin transport in the π -conjugated polymer poly(2,5-bis(3-alkylthiophen-2-yl)thiono[3,2-b]thiophene) (PBTTT) has been demonstrated to be governed by a SOC-mediated polaron hopping process¹². Therefore, spin diffusion is expected to obey the diffusion length

relation²⁹ $\lambda_S = \sqrt{DT_S}$, where λ_S is the spin diffusion length, D the charge carrier diffusion constant, and T_S is the spin relaxation time. On the contrary there are two theoretical models which predict that spin transport may be significantly more efficient than charge transport in OSEC films. One model claims that spin transport can be mediated by spin-exchange interaction in OSEC at high carrier concentration³⁰. The other model asserts that charge and spin transport may proceed in an impurity band that is effective in some areas in the film, where the spins interact via a long range antiferromagnetic coupling that is more beneficial to spin transport. This has been named as the two fluids model³¹.

In this work we report independent measurements of the spin diffusion and charge carrier diffusion in a number of disordered π -conjugated polymer films, among which is is the generic pristine polymer namely the Super Yellow *poly-phenylene-vinylene* (SY-PPV) (cf. Fig. 1a), using three different techniques: (i) Spin pumping in FM/SY-PPV/Pt trilayers for ISHE measurements for obtaining and the spin diffusion length; (ii) pulsed electrically detected magnetic resonance (EDMR) for measuring the transverse and longitudinal spin relaxation times; and (iii) time-of-flight experiments, for measuring the charge carrier mobilities. The independent experimental verification of these critical spin and charge transport parameters allow us to establish whether or not spin transport and charge transport in SY-PPV are governed by the same physical mechanisms.

The spin diffusion lengths in polymer thin films were measured using NiFe/polymer/Pt trilayer devices with various polymer thicknesses, as depicted schematically in Fig. 1b. The various devices were fabricated on glass substrates each with 7 nm Pt evaporated film over 30 nm thick Cu contact pads, followed by the polymer spin transport layer, and capped with 15 nm Ni₈₀Fe₂₀ (NiFe) spin injection layer. The polymer spin transport layers were spin-cast in N₂ atmosphere with casting speeds of 2000-7000 rpm in order to obtain different thicknesses *d*, and the finished trilayer devices were protected from oxidation by 100 nm SiO₂ capping layers. The surface morphology of the spin coated polymer films was characterized by atomic force microscopy, as shown in Fig. 1a. The roughness was estimated to be ~3nm for the SY-PPV thickness of ~150 nm; therefore, the magnetic properties of NiFe films deposited onto the various polymer films with different thicknesses are comparable. Additional details about the device structures and fabrication procedures can be found elsewhere ^{16,31}. For the ISHE measurements, the devices

Formatted: Font color: Auto

Formatted: Font color: Auto

Formatted: Font color: Auto

Formatted: Font color: Auto

were placed on a grounded co-planar waveguide (GCPW), which was mounted in an external magnetic field. FMR in the ferromagnetic (FM) layer was induced using microwave excitation with frequency f = 3 GHz and power $P \approx 1$ W. While the non-uniform B_1 field distribution generated by the co-planar waveguide prohibits determination of the absolute ISHE conversion strength³², it does allow for the comparison of relative ISHE magnitudes, assuming the B_1 distribution is similar in all samples; which was verified by reproducibility tests (within the measurement uncertainties) of the ISHE spectra.

Under FMR conditions, the FM NiFe film generates pure spin current at the NiFe/polymer interface which propagates into the polymer layer perpendicular to the interface. Once the spin current reaches the Pt detection layer on the opposite side of the device, it induces an ISHE current in the Pt film between the two Cu electrodes, which is oriented perpendicular to the spin polarization and spin current directions (i.e. parallel to the polymer/Pt surface). We note that the Pt layer (with resistance $R \sim 500~\Omega$) short-circuits the highly resistive polymer film; thus the observed emf signals can originate only from the ISHE within the Pt layer itself, and therefore represent spin diffusion through the full thickness of the polymer interlayer. The resulting ISHE voltage, $V_{\rm ISHE}$ was measured as a function of the applied static magnetic field B_0 over both positive and negative polarities (cf. Fig. 1c). Repeated measurements of such ISHE spectra (i. e. the measurement of $V_{\rm ISHE}$ as function of B_0) using devices with varying polymer layer thicknesses, d revealed the expected decrease of $V_{\rm ISHE}$ amplitude with increasing d.

In order to determine the spin relaxation time, $T_{\rm S}$ ($T_{\rm S}$ being equivalent to $T_{\rm 1}$ in spin pumping applications, with external field $B_{\rm 0}$ in-plane) of paramagnetic charge carriers in the SY-PPV polymer, we conducted pulsed EDMR spectroscopy using a Bruker Elexsys E580 pulse EPR spectrometer and a X-band Flexline MD5 resonator, following similar studies on other π -conjugated polymers in our laboratory^{33,34}. For these experiments, a bipolar injection thin-film device (an organic light emitting diode) was fabricated on a template which consisted of a transparent indium tin oxide (ITO) semitransparent anode, ~40 nm spin-cast polyethylenedioxythiophene:polystyrene sulphonate (PEDOT:PSS) hole transport and injection layer, ~200 nm SY-PPV interlayer, ~20 nm Ca electron transport layer, as well as ~100 nm aluminum capping layers that served as a cathode.

The measurement of T_1 was done using an inversion recovery pulse sequence, whereby a π -pulse is applied causing an inversion of the spin population in the device, which then is allowed to relax over time T. The recovered spin polarization is read out using a modified Hahn-echo sequence, which uses in addition to the standard $\pi/2-\tau-\pi-\tau$ pulse sequence (with $\pi/2$ pulses being ~ 10 ns long at 1 kW microwave power), another $\pi/2$ pulse for the projection of the rephased spin ensemble onto the permutation operator that is typically probed in EDMR experiments based on spin-dependent charge carrier recombination 35,36 . As shown in Fig. 2b, the magnitude of the electrically detected spin echo decreases with increasing T, allowing T_1 to be extracted from the decay. The transverse relaxation time T_2 was also found for the same device using a $\pi/2-\tau-\pi-\tau-\pi/2$ pulse sequence, which is a standard Hahn-echo sequence extended by the $\pi/2$ detection pulse T_1 is again extracted from the spin echo decay with increasing T, as shown in Fig. 2d.

Time-of-flight measurements devices of were carried out consisted on ITO/PEDOT:PSS/polymers/Ca/Al stacks as shown in Fig. 3a. Laterally, the devices had 2×2 mm² large active areas, while the measured thickness of the polymer layer was ~1 µm. Strong laser pulses (having 7 ns duration at 425 nm) were directed on the upper Al electrode, which was thin enough to allow for penetration into the underlying polymer layer. The laser pulses generated a thin layer of photo-excited species, including excitons and both positive and negative free carriers (polarons). By applying strong electric fields (~10⁶ V/cm) we observed diffusion of photocarriers across the polymer film thickness. Under reverse bias conditions, holes were swept from the Ca to the ITO layer, while electrons were blocked at the Ca interface due to its high work function. Transit times were extracted from the transient photocurrent measurements, from which the zero-field mobility could be calculated.

Figure 1c shows $V_{\text{ISHE}}(B)$ measured in the Pt layer in the trilayer structure NiFe/SY-PPV/Pt. The electric field direction is perpendicular to both the spin current and spin polarization directions¹³, $\vec{E}_{\text{ISHE}} \propto \vec{J}_{\text{S}} \times \vec{\sigma}$, where \vec{J}_{S} and $\vec{\sigma}$ are the spin current and spin polarization, respectively. The data display a sign inversion of the voltage at fields B with negative polarity, which is a signature behavior of the ISHE, showing that pure spin transport occurs through the polymer layer. As clearly seen in Fig. 1c, $V_{\text{ISHE}}(B)$ decreases with increasing polymer film thickness d; however, it

is still significant at d beyond 150 nm, demonstrating that this polymer is quite efficient as a spin transport medium. We exclude the possibility of contamination from magneto-galvanic effects, particularly the anisotropic magneto-resistance (AMR), in the NiFe layer due to the extremely high resistivity of the polymer spacer layer, found to be $\rho \sim 200~\Omega \text{m}^{38}$. The Pt detection layer, having resistance $R \sim 500~\Omega$, is essentially electrically isolated from any DC rectification voltage appearing across the NiFe layer. Figure 1d shows that the amplitude of $V_{\text{ISHE}}(B)$ as a function of d is nicely fit by an exponential decay, $V_{\text{ISHE}} \propto e^{-d/\lambda_{\text{S}}}$; where λ_{S} is the spin diffusion length of the SY-PPV polymer. From the fitting we obtain $\lambda_{\text{S}} = 39 \pm 6$ nm in SY-PPV.

The results of the spin echo measurements in SY-PPV film are shown in Fig. 2. The observed decay of the saturation recovery signal with increasing T, shown in panel b, is well-fit by a double exponential decay, with time constants of $29 \pm 1~\mu s$ and 3.8 μs . The longer time constant is consistent with T_1 times in conjugated polymers³⁴, and the shorter time constant is ascribed to an additional short-lived, spin-dependent species. As previously explained, we take T_1 to be the relevant spin decay lifetime that governs the spin diffusion process in the polymer layer, although we note that T_2 may also have significant correlation with the charge diffusion rates in certain materials^{39,40}. The decay of the T_2 spin echo response with increasing 2τ is shown in panel d, and is fit nicely by a stretched exponential of the form $\exp(-\tau/T_2)^{\beta}$, which gives $T_2 = 361 \pm 7$ ns with $\beta = 0.85$.

Figure 3b shows the transient photocurrent, $I_{PC}(t)$, of the time-of-flight measurements for SY-PPV based devices at increasing applied field strengths. Due to highly dispersive transport in the disordered polymer, $I_{PC}(t)$ follows a slow power-law decay, with a marked transition to a steeper decay once the initial excited carriers reach the other electrode⁴¹. The transition point or "kink" between the two power-law regions represents the transit time t_{tr} of the carriers across the film. From this 'kink' in the $I_{PC}(t)$ decay, the mobility μ can be calculated via the relationship $v_d = \mu F$, where v_d is the drift velocity and F the electric field; from which we obtain $\mu = L^2/t_{tr}V$, where L is the polymer layer thickness. The transit time t_{tr} is taken as the crossing point of the two power law fittings, at the visible shoulder in the response curves. The transit time is shorter at higher applied voltage due to the Poole-Frenkel effect. Transit time vs. applied field curves are shown for a SY-PPV film in Fig. 3c, with fits to the Poole-Frenkel equation and relevant parameters given. The calculated zero-field mobility is $\mu(0) = 1.5 \pm 0.3 \times 10^{-7}$ cm²/Vs. Based on

the Einstein relationship, the charge carrier diffusion coefficient $D_C = \mu k_B T/e$ can be estimated as $3.9 \pm 0.9 \times 10^{-9}$ cm²s⁻¹ for SY-PPV, where k_B is the Boltzmann factor.

The parameters measured with the different experimental techniques are summarized in Table I. From the measured spin relaxation time and spin diffusion length, we calculate the spin diffusion coefficient, $D_S = 5.2 \pm 1.6 \times 10^{-7} \text{ cm}^2 \text{s}^{-1}$ using the relation: $\lambda_S = \sqrt{D_S T_1}$. Also, from the carrier mobility measurement and the Einstein relationship, we derive the charge diffusion coefficient, $D_{\rm C} = 3.9 \pm 0.9 \times 10^{-9} \, {\rm cm}^2 {\rm s}^{-1}$. It is thus clear that the spin diffusion coefficient in SY-PPV is more than 100 time larger compared to the charge diffusion coefficient. The spin density in SY-PPV, as determined by electron spin resonance³⁸, is comparable to the charge carrier density; thus we exclude the possibility of artificial higher spin density in SY-PPV due to defects or unintentional doping during the sample preparations. We note that while the determination of D_S from the diffusion length revealed $D_S/D_C \approx 135$, under the assumption that the longitudinal spin relaxation time T_1 determines the spin diffusion lengths $^{42-46}$; this disparity becomes even greater if T_2 determines the spin diffusion lengths, i.e. if the ISHE was dependent on spin coherence rather than (classical) spin polarization memory⁴⁷. As a further check we also measured the mobility of SY-PPV by I-V characteristics with the same device configuration (Pt/SY-PPV/NiFe) as the ISHE devices; the charge carrier mobility is one order larger than that obtained by time of flight, but the discrepancy still exists. This discrepancy between spin diffusion and charge diffusion is too large to be explained away by simple experimental errors or uncertainties, and it is contrary to the recent finding that spin transport in doped polymers is mediated by polaron hopping, which would imply that spin transport would be due to the same mechanisms as charge transport¹².

To further verify the relation between spin and charge transport in disordered organic polymers, we also measured the spin and charge transport in various polymers, as summarized in Table I. The corresponding spin diffusion lengths and mobilities measurements results are shown in the S.M. Table I clearly demonstrates that there are always significant discrepancies between the spin and charge diffusion coefficients in disordered polymer films, in contrast to the comparable values of spin and charge diffusion coefficients in fullerene and its derivative. For the observed charge diffusion constants in disordered polymers, spin lifetimes of mobile charge carriers would need to exceed a few milliseconds¹² at room temperature to produce the observed spin diffusion

Formatted: Font color: Auto

Formatted: Font color: Auto

Formatted: Font color: Auto

lengths; therefore charge diffusion as the origin of spin diffusion appears to be entirely unrealistic. We thus deduce that the separation of spin and charge transport is quite common in disordered polymer films, in contrast to other OSEC, such as fullerenes.

Up to now, there are two theories predicting spin transport without involving charge motion in disordered OSCE^{30,31}: One is exchange mediated spin diffusion model that suggests an additional exchange coupling mechanism for spin transport in organic media Polarons in OSEC films can be delocalized over ~1 nm length scale, and, at high concentrations (> 10¹⁷ cm³), this may lead to an exchange interaction whereby carriers may communicate their spin-alignment to adjacent sites (which may not be charged) without physical hopping process. We note that this model has recently been experimentally verified by two different groups 42,48. The spin diffusions measured by spin valve and lateral spin pumping in small molecules and single crystal polymers both show increase with increasing the carrier densities. However, our experimental results cannot be directly explained by this model since direct exchange coupling cannot happen in pristine polymers with very low spin densities. The other model is the 'two fluids' model that proposes antiferromagnetic coupling between the spins of localized carriers from impurities acting as waves for spin transport in highly disordered polymer films³¹, whereas the delocalized carriers establish channel for charge transport. There are similarities for the two theoretical models, where the charge transport are both related to delocalized carriers hopping, but the difference is that spin transport proceeds through direct exchange coupling between spins of carriers in exchange mediated spin diffusion model instead of wave form in localized carriers with antiferromagnetic coupling for two fluids model. In our experiments, charge/spin densities are below the threshold of exchange mediated spin diffusion model, and in addition the disorder is much stronger in spin coated polymer films than in single crystals.

In conclusion, we have studied spin and charge transport in disordered conjugated polymer films, using three independent experimental techniques. These are: spin pumping and ISHE measurements in trilayer devices of NiFe/polymer/Pt; pulsed EDMR spectroscopy; and time-of-flight and I-V response measurements. From these measurements we have extracted the room temperature spin and charge diffusion constants of the pristine polymers. We found that the spin diffusion constant is significantly larger than the charge diffusion constant, indicating that the nature of spin and charge transport in disordered pristine polymer films, are fundamentally

Formatted: Font color: Auto

Formatted: Font color: Auto

different. We attribute the dominant spin transport mechanism in disordered OSEC to the recent developed 'two fluids' model. These findings deepen our understanding of spin transport in disordered OSEC with strongly localized electronic states. Combined with recent reports of exchange interaction dominant spin diffusion in highly doped polymers $^{42}_{\bullet}$, we conclude that spin transport in π -conjugated polymers may proceed by wave propagation from antiferromagnetic coupling or direct spin-spin exchange interaction, separated from charge transport by hopping.

Formatted: Font color: Auto
Formatted: Font color: Auto
Formatted: Font color: Auto
Formatted: Font color: Auto

<u>Acknowledgments</u>: This work was supported by the National Science Foundation grant (DMR-1701427).

References

- ¹ J.H. Burroughes, D.D.C. Bradley, A.R. Brown, R.N. Marks, K. Mackay, R.H. Friend, P.L. Burns, and A.B. Holmes, Nature **347**, 539 (1990).
- ² S. Kubatkin, A. Danilov, M. Hjort, J. Cornil, J.-L. Brédas, N. Stuhr-hansen, P. Hedegård, and T. Bjørnholm, Nature **425**, 698 (2003).
- ³ A.J. Heeger, Adv. Mater. **26**, 10 (2014).
- ⁴ Z.H. Xiong, D. Wu, Z.V. Vardeny, and J. Shi, Nature **427**, 821 (2004).
- ⁵ V.A. Dediu, L.E. Hueso, I. Bergenti, and C. Taliani, Nat. Mater. **8**, 707 (2009).
- ⁶ C. Barraud, P. Seneor, R. Mattana, S. Fusil, K. Bouzehouane, C. Deranlot, P. Graziosi, L. Hueso, I. Bergenti, V. Dediu, F. Petroff, and A. Fert, Nat. Phys. **6**, 615 (2010).
- ⁷ M. Gobbi, A. Bedoya-Pinto, F. Golmar, R. Llopis, F. Casanova, and L.E. Hueso, Appl. Phys. Lett. **101**, 102404 (2012).
- ⁸ M.C. Wheeler, F. Al Ma'Mari, M. Rogers, F.J. Gonçalves, T. Moorsom, A. Brataas, R. Stamps, M. Ali, G. Burnell, B.J. Hickey, and O. Cespedes, Nat. Commun. **8**, 926 (2017).
- ⁹ M. Gobbi, F. Golmar, R. Llopis, F. Casanova, and L.E. Hueso, Adv. Mater. **23**, 1609 (2011).
- ¹⁰ H. Liu, J. Wang, M. Groesbeck, X. Pan, C. Zhang, and Z. Vardeny, J. Mater. Chem. C **6**, 3621 (2018).
- ¹¹ V. Dediu, M. Murgia, F.C. Matacotta, C. Taliani, and S. Barbanera, Solid State Commun. **122**, 181 (2002).
- ¹² S. Watanabe, K. Ando, K. Kang, S. Mooser, Y. Vaynzof, H. Kurebayashi, E. Saitoh, and H. Sirringhaus, Nat. Phys. **10**, 308 (2014).
- ¹³ E. Saitoh, M. Ueda, H. Miyajima, and G. Tatara, Appl. Phys. Lett. **88**, 182509 (2006).
- ¹⁴ K. Ando, S. Watanabe, S. Mooser, E. Saitoh, and H. Sirringhaus, Nat. Mater. 12, 622 (2013).
- ¹⁵ Z. Qiu, M. Uruichi, D. Hou, K. Uchida, H.M. Yamamoto, and E. Saitoh, AIP Adv. 5, (2015).

- ¹⁶ D. Sun, K.J. Van Schooten, M. Kavand, H. Malissa, C. Zhang, M. Groesbeck, C. Boehme, and Z. Valy Vardeny, Nat. Mater. **15**, 863 (2016).
- ¹⁷ S.W. Jiang, S. Liu, P. Wang, Z.Z. Luan, X.D. Tao, H.F. Ding, and D. Wu, Phys. Rev. Lett. **115**, 086601 (2015).
- ¹⁸ M. Kimata, D. Nozaki, Y. Niimi, H. Tajima, and Y. Otani, Phys. Rev. B **91**, 224422 (2015).
- ¹⁹ Y. Tani, T. Kondo, Y. Teki, and E. Shikoh, Appl. Phys. Lett. **110**, 032403 (2017).
- ²⁰ J.B.S. Mendes, O. Alves Santos, J.P. Gomes, H.S. Assis, J.F. Felix, R.L. Rodríguez-Suárez, S.M. Rezende, and A. Azevedo, Phys. Rev. B 95, 014413 (2017).
- ²¹ H. Liu, M. Groesbeck, E. Lafalce, X. Liu, and Z.V. Vardeny, J. Photonics Energy **8**, 032212 (2018).
- ²² S. Sanvito, Nat. Phys. **6**, 562 (2010).
- ²³ M. Cinchetti, V.A. Dediu, and L.E. Hueso, Nat. Mater. **16**, 507 (2017).
- ²⁴ V. Coropceanu, J. Cornil, D.A. da Silva Filho, Y. Olivier, R. Silbey, and J.-L. Brédas, Chem. Rev. **107**, 926 (2007).
- ²⁵ T.D. Nguyen, G. Hukic-Markosian, F. Wang, L. Wojcik, X.G. Li, E. Ehrenfreund, and Z.V. Vardeny, Nat. Mater. **9**, 345 (2010).
- ²⁶ P.A. Bobbert, W. Wagemans, F.W.A. Van Oost, B. Koopmans, and M. Wohlgenannt, Phys. Rev. Lett. **102**, 156604 (2009).
- ²⁷ Z.G. Yu, Phys. Rev. Lett. **106**, 106602 (2011).
- ²⁸ S. Schott, E.R. McNellis, C.B. Nielsen, H.-Y. Chen, S. Watanabe, H. Tanaka, I. McCulloch, K. Takimiya, J. Sinova, and H. Sirringhaus, Nat. Commun. 8, 15200 (2017).
- ²⁹ A. Einstein, *Investigations on the Theory of the Brownian Movement* (Courier Corporation, 1956).
- ³⁰ Z.G. Yu, Phys. Rev. Lett. **111**, 016601 (2013).

³¹ H. Liu, C. Zhang, H. Malissa, M. Groesbeck, M. Kavand, R. McLaughlin, S. Jamali, J. Hao, D. Sun, R.A. Davidson, L. Wojcik, J.S. Miller, C. Boehme, and Z.V. Vardeny, Nat. Mater. **17**, 308 (2018).

- ³² M. Kavand, C. Zhang, D. Sun, H. Malissa, Z. V. Vardeny, and C. Boehme, Phys. Rev. B **95**, 161406(R) (2017).
- ³³ R. Miller, K.J. Van Schooten, H. Malissa, G. Joshi, S. Jamali, J.M. Lupton, and C. Boehme, Phys. Rev. B **94**, 214202 (2016).
- ³⁴ W.J. Baker, T.L. Keevers, J.M. Lupton, D.R. McCamey, and C. Boehme, Phys. Rev. Lett. **108**, 267601 (2012).
- ³⁵ D.R. McCamey, H.A. Seipel, S.-Y. Paik, M.J. Walter, N.J. Borys, J.M. Lupton, and C. Boehme, Nat. Mater. 7, 723 (2008).
- ³⁶ H. Malissa, M. Kavand, D.P. Waters, K.J. van Schooten, P.L. Burn, Z. V. Vardeny, B. Saam, J.M. Lupton, and C. Boehme, Science **345**, 1487 (2014).
- ³⁷ H. Huebl, F. Hoehne, B. Grolik, A.R. Stegner, M. Stutzmann, and M.S. Brandt, Phys. Rev. Lett. **100**, 177602 (2008).
- ³⁸ See Supplemental Material at [link inserted by publisher] for extensive details about the electrical device characterization and spin density measurements.
- ³⁹ K. Marumoto, N. Arai, H. Goto, M. Kijima, K. Murakami, Y. Tominari, J. Takeya, Y. Shimoi, H. Tanaka, S. Kuroda, T. Kaji, T. Nishikawa, T. Takenobu, and Y. Iwasa, Phys. Rev. B **83**, 075302 (2011).
- ⁴⁰ M.Y. Teferi, J. Ogle, G. Joshi, H. Malissa, S. Jamali, D.L. Baird, J.M. Lupton, L. Whittaker Brooks, and C. Boehme, Phys. Rev. B 98, 241201(R) (2018).
- ⁴¹ H. Scher and E.W. Montroll, Phys. Rev. B **12**, 2455 (1975).
- ⁴² S.-J. Wang, D. Venkateshvaran, M.R. Mahani, U. Chopra, E.R. McNellis, R. Di Pietro, S. Schott, A. Wittmann, G. Schweicher, M. Cubukcu, K. Kang, R. Carey, T.J. Wagner, J.N.M. Siebrecht, D.P.G.H. Wong, I.E. Jacobs, R.O. Aboljadayel, A. Ionescu, S.A. Egorov, S. Mueller,

- O. Zadvorna, P. Skalski, C. Jellett, M. Little, A. Marks, I. McCulloch, J. Wunderlich, J. Sinova, and H. Sirringhaus, Nat. Electron. **2**, 98 (2019).
- ⁴³ Z.G. Yu, Phys. Rev. B Condens. Matter Mater. Phys. **85**, 115201 (2012).
- ⁴⁴ J. Rawson, P.J. Angiolillo, P.R. Frail, I. Goodenough, and M.J. Therien, J. Phys. Chem. B **119**, 7681 (2015).
- ⁴⁵ N. Tombros, C. Jozsa, M. Popinciuc, H.T. Jonkman, and B.J. Van Wees, Nature **448**, 571 (2007).
- ⁴⁶ Y. Fukuma, L. Wang, H. Idzuchi, S. Takahashi, S. Maekawa, and Y. Otani, Nat. Mater. **10**, 527 (2011).
- ⁴⁷ J. Tsurumi, H. Matsui, T. Kubo, R. Häusermann, C. Mitsui, T. Okamoto, S. Watanabe, and J. Takeya, Nat. Phys. **13**, 994 (2017).

Table I. Summary of spin and charge transport parameters for SY-PPV polymer films.

Table I. Summary of spin and charge transport parameters for P3HT and SY-PPV OSC polymers.

Material	T_2	T_1	μ	$N_{\mathbf{c}}$	$\lambda_{ m S}$	$\mathbf{D}_{\mathbf{C}}$	D _S	Formatted: Font: Bold
								Formatted: Font: Bold
	(ns)	(µs)	$(10^{-7} \text{cm}^2 \text{V}^-)$	(10 ¹⁶ cm	(nm)	$(10^{-7} \text{cm}^2 \text{s}^{-1})$	(10 ⁻⁷ cm ² s ⁻	Formatted: Font: Bold
			¹ s ⁻¹).	³).				Formatted: Font: Bold
] 	Formatted: Font: Bold
SY-PPV.	360± 7	29 ± 1	1.5 ± 0.1	0.7 ± 0.2	39± 6	0.039 ±	5.2 ± 1.6	Formatted: Font: Bold
								Formatted: Font: Bold
						0.009	\	Formatted: Font: Bold
DATE	50	0.56	120	1 2 . 0 2	22 + 5	2.004	060+60	Formatted: Font: Bold
РЗНТ	50-	0.56	120	1.2 ± 0.2	22± 5	3.084	968 ± 60	Formatted: Font: Bold
	200*						\ \\	Formatted: Font: Bold
							\ \/	Formatted: Font: Bold
PC ₇₀ BM ¹⁶		140	~10000		66±8	~257	31.2±0.4	Formatted: Font: Bold
							\ \	Formatted: Font: Bold
Polyfluorene ^{28,38}	253±	5	31±3		118±9	0.796±	278.5 ± 16.2	Formatted: Font: Bold
_	82					0.008	7 / //	Formatted: Font: Bold
	02					0.008	\	Formatted: Font color: Auto
C70 ^{10,39}		0.1.1	6500	0.10	17+2	167	280	Formatted: Font: Bold, Font color: Auto
C/U		0.1-1	6500	0.10-	17±2	167	289	Formatted: Font color: Auto
				3.12			\ \	Formatted: Font color: Auto
								Formatted: Font: Bold
								Formatted: Font: Bold
								Formatted: Font: Bold

FIGURES

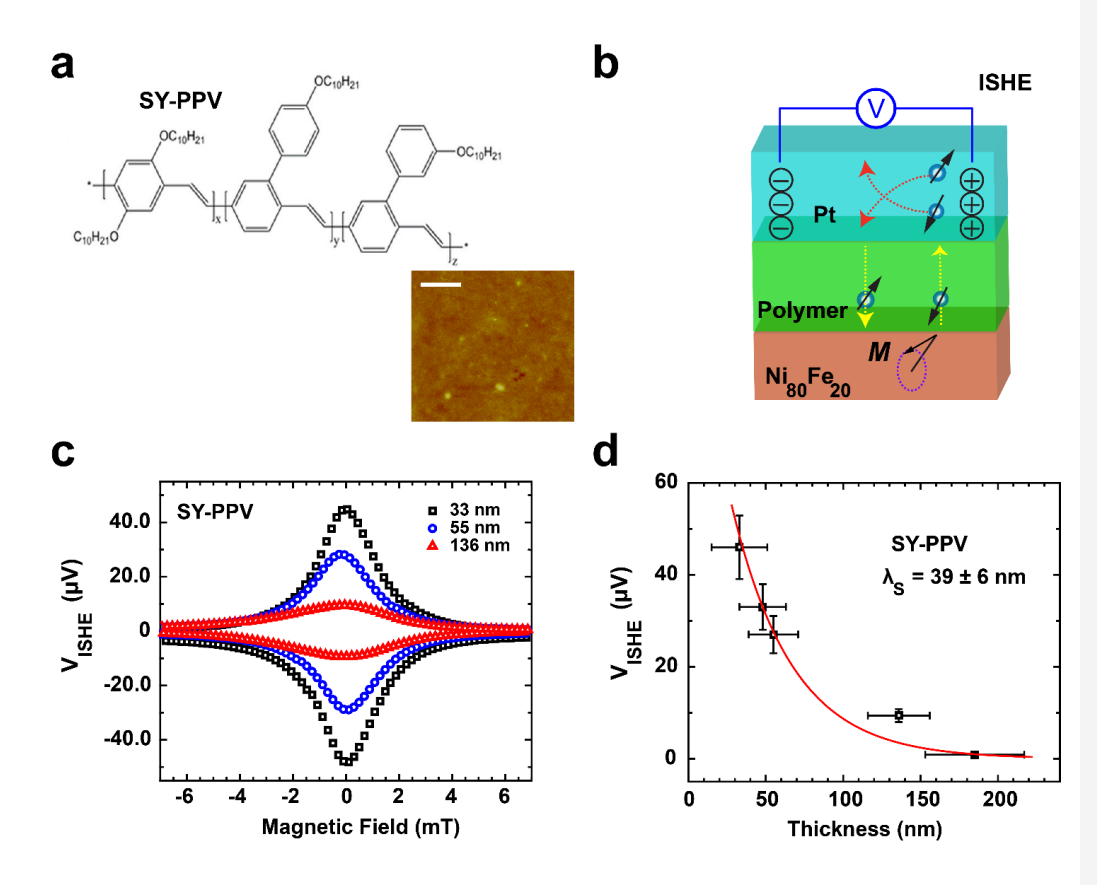


Figure 1. Measurement of the spin diffusion length in the polymer SY-PPV using NiFe/polymer/Pt trilayer devices with various polymer thicknesses, d and spin pumping/ISHE experiments. (a) SY-PPV molecular structure and surface morphology of ~ 150 nm thickness film deposited on Pt, measured by atomic force microscopy. The white bar is 4 μm. (b) Schematics of the spin pumping process in the trilayer structure as explained in the text. (c) The ISHE voltage, $V_{\rm ISHE}(B)$ response generated in the Pt layer in trilayer devices with various d. (d) SY-PPV thickness dependence of the $V_{\rm ISHE}$ amplitude. The $V_{\rm ISHE}$ decay with d is fit with an exponential function to extract the room-temperature spin diffusion length, $λ_{\rm S}$ in SY-PPV.

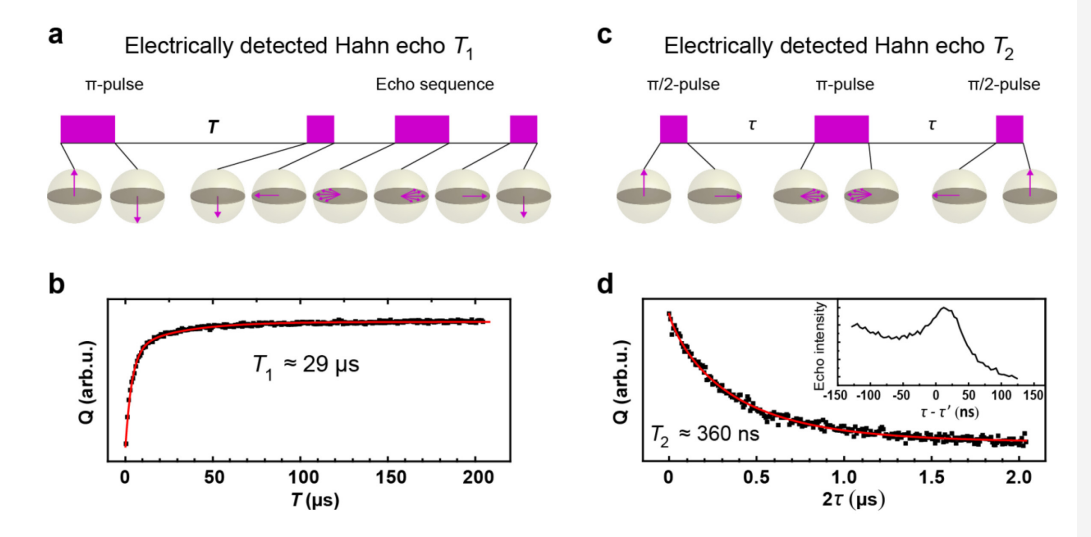


Figure 2. Spin lifetimes in SY-PPV measured with EDMR spectroscopy. (a) Schematic of the electrically detected saturation recovery measurements. (b) Plot of the recovery signal amplitude as a function of saturation time, T. (c) Schematic of the electrically detected Hahn echo measurements, which deviate from inductively detected Hahn-echo sequences through the readout pulse which projects spin polarization onto the permutation symmetry operator that is probed in EDMR experiments³⁵. (d) Plot of the Hahn-echo amplitude as a function of 2τ . Inset: a typical EDMR detected echo signal. By fitting the decays in (b) and (d), the spin relaxation times T_1 and T_2 are obtained, respectively.

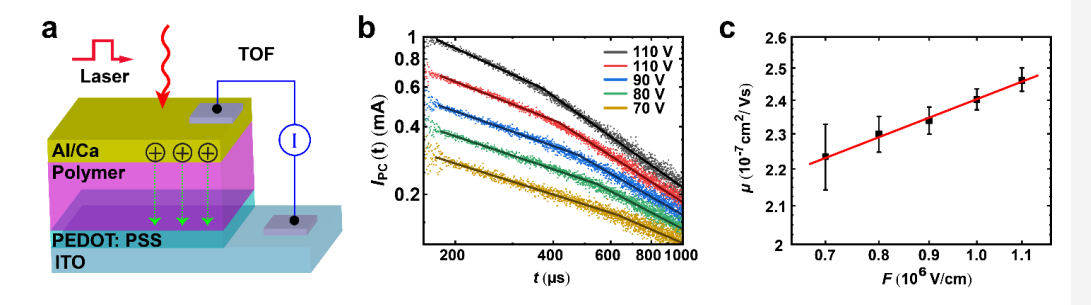


Figure 3. Charge carrier mobility measurements in SY-PPV film using the time-of-flight (TOF) method. (a) Schematics of the TOF measurement. (b) TOF transient photocurrent decay I_{PC} with double logarithmic plots, showing typical dispersive transport in the film. The measurements were done at room temperature with effective electric fields of approximately 10^6 V/cm. (c) Electric bias field dependence of the TOF mobilities in SY-PPV. The solid line is fit by the Poole-Frenkel equation.